

# **Random Sampling High Dimensional Model Representation**

## **Gaussian Process Regression (RS-HDMR-GPR): a Python module**

### **for representing multidimensional functions with machine-learned**

### **lower-dimensional terms**

Owen Ren,<sup>a,b</sup> Mohamed Ali Boussaidi,<sup>a,c</sup> Dmitry Voitsekhovsky,<sup>b</sup> and Sergei Manzhos<sup>a,1</sup>

<sup>a</sup> Centre Énergie Matériaux Télécommunications, Institut National de la Recherche Scientifique,  
1650 boulevard Lionel-Boulet, Varennes QC J3X1S2 Canada.

<sup>b</sup> Purefacts Inc., 48 Yonge St Suite 400, Toronto, ON M5E 1G6 Canada.

<sup>c</sup> Ecole Nationale d'Ingénieurs de Tunis, Rue Béchir Salem Belkhiria Campus universitaire, BP  
37, 1002, Le Bélvédère, Tunis, Tunisia.

## **Abstract**

We present a Python implementation for RS-HDMR-GPR (Random Sampling High Dimensional Model Representation Gaussian Process Regression). The method builds representations of multivariate functions with lower-dimensional terms, either as an expansion over orders of coupling or using terms of only a given dimensionality. This facilitates, in particular, recovering functional dependence from sparse data. The code also allows imputation of missing values of the variables. The capabilities of this regression tool are demonstrated on test cases involving synthetic analytic functions, the potential energy surface of the water molecule, and financial market data.

**Keywords:** multivariate function, machine learning, Gaussian process regression, High Dimensional Model Representation, data imputation.

## **PROGRAM LINK**

<https://github.com/owen-ren0003/rshdmrgpr>

---

<sup>1</sup> Corresponding author. E-mail: sergei.manzhos@emt.inrs.ca

## 1 Introduction

Interpolation or fitting of a multivariate function  $f(\mathbf{x}), \mathbf{x} \in R^D$  from discrete samples  $\{\mathbf{x}^{(j)}\}, j = 1, 2, \dots, M$  is a ubiquitous problem in natural sciences and beyond. In high-dimensional spaces (with dimensionality  $D$  of more than about 6) this problem is difficult enough so that standard approaches such as polynomial interpolation, splines or direct product basis expansions (e.g. Fourier expansion) often fail. This has to do, in particular, with an exponential growth of the required numbers of sampled values and of terms in direct product type representations. These numbers quickly become impractical as  $D$  is increased; this is known as the “curse of dimensionality”.<sup>1</sup> The sampling of functions in high-dimensional spaces is necessarily sparse; for example, 100,000 samples in a 20-dimensional space is equivalent to about 1.8 points per dimension of a direct product grid. Increasing the number of data to 1,000,000 would only result in a density of sampling increase to about 2 points per dimension. Methods are therefore required that can work with sparse samples. Further, the distribution of sampled data may be arbitrary, and data, especially those corrected during observation of physical, social etc. phenomena, do not generally lie on a grid and are not distributed in any particular way. Methods are therefore required which can work with any data distribution. It is clear from the above that in high-dimensional spaces non-direct product approaches need to be used. Machine learning approaches such as neural networks (NN)<sup>2, 3</sup> or Gaussian process regression (GPR)<sup>4</sup> used in the present work are examples of such representations which in this sense avoid the exponential scaling of the cost (both in terms of required data and in terms of required number of terms in the representation) with dimension.

Even with machine learning methods, the problem of reconstructing functional dependence from sparse, arbitrarily distributed samples in multidimensional spaces is difficult. For example, the number of required data and neurons of an NN may be large and lead to overfitting even as NNs can handle millions of data,<sup>5, 6</sup> while the cost of GPR becomes problematic with more than about 5,000 data points (due to the need to operate with a matrix of size  $M \times M$  and respective matrix-vector products). A useful approach that leverages the capability of ML methods is representation of a multidimensional function with lower-dimensional terms. Rabitz et al. introduced High Dimensional Model representation (HDMR)<sup>7-9</sup> which is an expansion over orders of coupling:

$$f(\mathbf{x}) \approx f_0 + \sum_{i=1}^D f_i(x_i) + \sum_{1 \leq i < j \leq D} f_{ij}(x_i, x_j) + \cdots + \sum_{\{i_1 i_2 \dots i_d\} \in \{12 \dots D\}} f_{i_1 i_2 \dots i_d}(x_{i_1}, x_{i_2}, \dots, x_{i_d}) \quad (1)$$

where  $d \leq D$  is the maximum order of coupling considered. The ANOVA decomposition<sup>10, 11</sup> used in data analysis and the many-body and multimode approximations<sup>12-16</sup> used in computational chemistry are particular cases of HDMR. In many practically important applications, using terms with  $d \leq 3$  is often sufficient.<sup>7</sup> Moreover, when sampling is sparse, only low-dimensional component functions can be reliably recovered.<sup>17, 18</sup> Fitting/interpolation of a lower-dimensional component function  $f_{i_1 i_2 \dots i_d}(x_{i_1}, x_{i_2}, \dots, x_{i_d})$ ,  $d < D$ , in particular with ML methods, is in principle an easier task than constructing the full-dimensional  $f(\mathbf{x})$ . A representation with lower-dimensional functions is also advantageous when using the function, in particular, if  $f(\mathbf{x})$  needs to be integrated.

One advantage of HDMR as introduced by Rabitz et al. (as well as of the ANOVA and multimode representations) is orthogonality of its component functions  $f_{i_1 i_2 \dots i_d}(x_{i_1}, x_{i_2}, \dots, x_{i_d})$ :

$$\int_D w(\mathbf{x}) f_{i_1 i_2 \dots i_d}(x_{i_1}, x_{i_2}, \dots, x_{i_d}) f_{j_1 j_2 \dots j_m}(x_{j_1}, x_{j_2}, \dots, x_{j_m}) d\mathbf{x} = 0 \quad \{i_1, i_2, \dots, i_d\} \neq \{j_1, j_2, \dots, j_m\} \quad (2)$$

when  $w(\mathbf{x}) = \prod_{i=1}^D w_i(x_i)$ , where  $w(\mathbf{x})$  is the weight function. If the data are distributed (e.g. randomly) in the  $D$ -dimensional space (as opposed to being constrained to  $d$ -dimensional hypersurfaces<sup>7, 9</sup>), the component functions of the resulting Radom Sampling (RS-) HDMR<sup>19, 20</sup> can all be determined from one and the same dataset and are defined via multidimensional integrals, specifically,  $(D - d)$  dimensional for  $d$ -dimensional component functions. The integrals approach is obviously impractical for high  $D$ .<sup>8, 19-21</sup> We introduced a generalization of HDMR whereby  $f(\mathbf{x})$  is approximated as<sup>17, 18, 22</sup>

$$f(\mathbf{x}) \approx \sum_{\{i_1 i_2 \dots i_d\} \in \{12 \dots D\}} f_{i_1 i_2 \dots i_d}(x_{i_1}, x_{i_2}, \dots, x_{i_d}) \quad (3)$$

i.e. as a sum of lower-dimensional functions of any given dimensionality  $d < D$ , where the component functions are each fitted in cycles as

$$f_{k_1 k_2 \dots k_d}(x_{k_1}, x_{k_2}, \dots, x_{k_d}) = f(\mathbf{x}) - \sum_{\substack{\{i_1 i_2 \dots i_d\} \in \{12 \dots D\} \\ \{i_1 i_2 \dots i_d\} \neq \{k_1 k_2 \dots k_3\}}} a(c) f_{i_1 i_2 \dots i_d}(x_{i_1}, x_{i_2}, \dots, x_{i_d}) \quad (4)$$

with a generic algorithm like NN or GPR.<sup>17, 18, 22</sup> The factor  $a(c)$ , where  $c$  is the cycle number, is introduced to prevent “crowding out” by the first fits of the fits of other component functions (which may happen, in particular, because of the non-unique way in which lower order terms of Eq. 1 can be subsumed into  $d$ -dimensional terms of Eq. 3), which may lead to the algorithm getting stuck in a local minimum.<sup>18</sup> One starts with  $0 < a(0) < 1$  and brings  $a(c)$  to 1 over a number of cycles. This approach does not ensure orthogonality of component functions but gains in simplicity. Specifically, one completely dispenses with the need to compute multi-dimensional integrals, and any distribution of data in  $D$ -dimensional space can be used. Building a full expansion over orders of coupling (e.g. if one desires access separately to  $f_i(x_i)$  and  $f_{ij}(x_i, x_j)$ ) is also possible based on Eq. 3, in which case one could fit

$$f_{k_1 k_2 \dots k_d}(x_{k_1}, x_{k_2}, \dots, x_{k_d}) = T(\mathbf{x}) - \sum_{\substack{\{i_1 i_2 \dots i_d\} \in \{12 \dots D\} \\ \{i_1 i_2 \dots i_d\} \neq \{k_1 k_2 \dots k_3\}}} a(c) f_{i_1 i_2 \dots i_d}(x_{i_1}, x_{i_2}, \dots, x_{i_d}) \quad (5)$$

where

$$\begin{aligned} T(\mathbf{x}) = f(\mathbf{x}) - & \left( f_0 + \sum_{i=1} f_i(x_i) + \sum_{1 \leq i < j \leq D} f_{ij}(x_i, x_j) + \dots \right. \\ & \left. + \sum_{\{i_1 i_2 \dots i_{d-1}\} \in \{12 \dots D\}} f_{i_1 i_2 \dots i_{d-1}}(x_{i_1}, x_{i_2}, \dots, x_{i_{d-1}}) \right) \end{aligned}$$

Alternatively, one can fit terms of different dimensionality simultaneously, which is the implementation we use, see section 2.1.

The classic HDMR expansion has recently been combined with GPR in specific applications.<sup>23</sup>

<sup>24</sup> The code presented here implements Eq. 3 where the component functions  $f_{i_1 i_2 \dots i_d}(x_{i_1}, x_{i_2}, \dots, x_{i_d})$  are represented with Gaussian process regression models and is therefore called RS-HDMR-GPR. The reader is referred to the literature<sup>4</sup> for a description of the GPR method which will not be repeated here. GPR<sup>4</sup> is a powerful technique that has been shown to outperform NNs in accuracy and/or required number of data to achieve a given accuracy. In fact, it is the only ML regression technique that has been shown to do so in *controlled* comparisons.<sup>25</sup>

<sup>26</sup> We have recently shown that RS-HDMR-GPR can provide highly accurate fits to sparse multidimensional data when fitting molecular potential energy surfaces used, in particular, to compute highly accurate vibrational spectra, which is a very stringent test.<sup>18</sup>

Another issue that we address with our code are missing values. The problem of missing data plagues data analysis. Assuming that data are given in the form  $\{\mathbf{X}, \mathbf{Y}\}$ , where  $\mathbf{X}$  is a  $M \times D$  matrix of  $M$   $D$ -dimensional inputs and  $\mathbf{Y}$  is a  $M \times 1$  vector of  $M$  output values, we define here missing data as elements of  $\mathbf{X}$  of which the values are unknown. We assume that all the rows of the target  $\mathbf{Y}$  are known. The origins of missing data are multiple and ubiquitous. For example, in financial markets data considered below, different trading days for different ticker symbols (such as stocks or indices from different jurisdictions) result in some incomplete rows of  $\mathbf{X}$  if  $i$  indexes trading days. In clinical data, as another example, one often aggregates data from many hospitals (as any given hospital often does not have a statistically significant record on a given disease or drug) where some values (patient / test data or various symptoms or reactions to a drug) are recorded and some are not depending on the hospital or on jurisdiction. The resulting combined data set can have large amounts of missing data.

In some cases, the missing values can be handled relatively painlessly. For example, in financial markets data, even when retaining only complete data rows, most of the data would be preserved. Interpolating values on trading holidays is also reasonable. In other cases, including the clinical data example above, this cannot be done. Retaining only the complete rows risks in many cases losing most of the data even if only a small fraction of  $\mathbf{X}$  entries is missing as long as many rows have at least one missing value. For example, if one collects 10,000 50-dimensional instances

for a total of 500,000 entries of  $\mathbf{X}$ , when as few as 1% of entries are missing, retaining only complete rows would result in discarding up to half of the data if the missing values are spread across the rows and column evenly (if the missing values are concentrated in certain columns, one can instead discard the variables); 2% of missing entries could make discard all of the data! This is a major issue with relatively little offered by way of remedies. The popular approach of imputing missing values based on data distribution<sup>27</sup> is masking rather than solving the problem.

The RS-HDMR-GPR code allows for reliable imputation of missing values for a specific case of one missing value per row of  $\mathbf{X}$  when the quality of the uncoupled approximation ( $d = 1$ ) is reasonable and the component functions are well-behaved.

## 2 The algorithm

### 2.1 RS-HDMR-GPR algorithm

The algorithm works as follows: given a feature matrix  $\mathbf{X}$  of dimension  $M \times D$ , we specify  $N$  matrices  $\mathbf{A}_1, \mathbf{A}_2, \dots, \mathbf{A}_N$  each with  $D$ -rows, where  $N$  is the number of the component functions (i.e.  $N = C_d^D$ , where  $C_d^D$  is the binomial coefficient). These matrices are used to select the inputs for the HDMR component functions by right multiplication with  $\mathbf{X}$ . For instance, if we wanted the component function inputs for  $d = 1$  (the one-dimensional HDMR) for a  $M \times 3$  feature matrix  $\mathbf{X}$ , then we define

$$\mathbf{A}_1 = \begin{pmatrix} 1 \\ 0 \\ 0 \end{pmatrix}, \quad \mathbf{A}_2 = \begin{pmatrix} 0 \\ 1 \\ 0 \end{pmatrix}, \quad \mathbf{A}_3 = \begin{pmatrix} 0 \\ 0 \\ 1 \end{pmatrix}, \quad (7)$$

and the resulting matrix product  $\mathbf{X}\mathbf{A}_i$  will yield the  $i$ -th column of  $\mathbf{X}$  as the input for the  $i$ -th HDMR component function for  $i = 1, 2, 3$ . The inputs are produced similarly for  $d > 1$ , in which case we would need more than one column and 1's entered to the matrices  $\mathbf{A}_n$ , as shown below. Note that this way of selecting inputs is not just limited to selecting columns. By filling the matrix  $\mathbf{A}$  with other values, we may select any linear combinations of columns of  $\mathbf{X}$  for each components input; an example of this is also given in section 3. Also possible with this type of fitting are the mixing of components of different dimension. For example, for the same above example of a  $M \times 3$  feature matrix  $\mathbf{X}$ , we can define

$$\mathbf{A}_1 = \begin{pmatrix} 1 \\ 0 \\ 0 \end{pmatrix}, \mathbf{A}_2 = \begin{pmatrix} 0 \\ 1 \\ 0 \end{pmatrix}, \mathbf{A}_3 = \begin{pmatrix} 0 \\ 0 \\ 1 \end{pmatrix}, \mathbf{A}_4 = \begin{pmatrix} 1 & 0 \\ 0 & 1 \\ 0 & 0 \end{pmatrix}, \mathbf{A}_5 = \begin{pmatrix} 1 & 0 \\ 0 & 0 \\ 0 & 1 \end{pmatrix}, \mathbf{A}_6 = \begin{pmatrix} 0 & 0 \\ 1 & 0 \\ 0 & 1 \end{pmatrix} \quad (8)$$

which will result in fitting all component functions of the approximation  $f(\mathbf{x}) = \sum_{i=1}^D f_i(x_i) + \sum_{1 \leq i < j \leq D} f_{ij}(x_i, x_j)$  simultaneously. The user may also decide to use only subsets of component function of a given dimension. The choice of which matrices are used is controlled by the user with the only restriction that each matrix must have number of rows equal to  $M$  and number of columns less than or equal to  $D$ .

With the inputs of the component functions defined, the individual GPR models representing the component functions are trained one at a time for  $i = 1, 2, \dots, N$  and in this specified order (the order itself is not important). This training is repeated for a number of cycles (which by default is set to 50) until the output of each component function has converged over the cycles. A priori it is not known how many cycles it would take for convergence, and this part must be determined empirically by trying various number of cycles. Usually when  $N$  is big, more cycles are needed. To prevent crowding out of component functions as described above, the first several cycles use only a percentage of the output as the fit target and slowly across cycles, that percentage is increased to 100. The increase happens linearly until this percentage reaches 100. The rate of increase is controlled by parameters from the *predict* function (see page 2 of the manual). Note that we did not necessarily have to define the increase linearly, any function that monotonically increases reasonably would have worked. We picked a linear function for simplicity. Denote by  $a(c)$  this growth function as a function of the current cycle  $c$ . Initially, we set the outputs (labels) of all the component function outputs to the vector  $\mathbf{Y}/N$ . Following that, we fit each component function  $f_{i_1 i_2 \dots i_d}$  for all  $\{i_1 i_2 \dots i_{d-1}\} \in \{1 2 \dots D\}$  one at a time as per Eq. 4. When a  $f_{i_1 i_2 \dots i_d}$  is fit, we replace the output of  $f_{i_1 i_2 \dots i_d}$  by  $a(c)f_{i_1 i_2 \dots i_d}$  and continue with the next fit. In the code, we defined  $a(c)$  by:

$$a(c) := \max \left\{ s + \frac{(1-s)ec}{C}, 1 \right\} \quad (9)$$

where  $s, e$  are specified parameters,  $c$  is the current cycle and  $C$  is the total number of cycles. The final output of the model is returned as the sum of these component functions. There is also the

option of returning the standard deviation of the estimate of  $f(\mathbf{x})$  computed as a square root of the sum of the variances of the component functions, where for the GPR of each component function the variance is given by

$$\Delta f_{i_1 i_2 \dots i_d}(x_{i_1}, x_{i_2}, \dots, x_{i_d}) = K^{**} - \mathbf{K}^* \mathbf{K}^{-1} \mathbf{K}^{*T} \quad (10)$$

Note that Eq. 10 computed the *confidence* of the expectation value of the component function computed by GPR. It is not a number indicative of the quality of the fit. For example, the confidence interval estimated with Eq. 10 will in general be higher in a full-dimensional fit than with HDMR with a low  $d$ , even if the RMSE of the fit is higher with a low- $d$  model. An example is given in Supporting Information (Figure S3). This is natural, as the values of component functions of the first-order HMDR model are more reliably estimated even with fewer data, even if the 1d-HDMR-GPR model overall has a higher fit RMSE due to the neglect of coupling. Values returned by Eq. 10 should therefore not be used as error bars on the fitted values. This is true in any GPR fit, for example, adding Gaussian noise with zero mean to the data will not, as long as data are abundant, make less reliable the estimates of *the expectation values* of  $f(\mathbf{x})$  even though such values will be much different from the data due to the noise, resulting in a higher RMSE.

## 2.2 Handling of missing data

The HDMR structure allows smarter imputation of missing data. We will consider a single-dimensional output  $\mathbf{Y}$ ,  $y_m = f(\mathbf{x}_m)$ , and consider first a specific case where a single missing value may occur in a row. This will be an easier to handle case with HDMR but, as shown in the example above, for a given fraction of missing entries, this seemingly simple case represents the worst case scenario if one has to retain only complete rows. Consider a first-order HDMR approximation

$$f(\mathbf{x}) \approx f_0 + \sum_{i=1}^D f_i(x_i) \quad (11)$$

As shown previously,<sup>18, 28</sup> low-order component functions require fewer data to be well-defined. Specifically, first-order component functions require the fewest data to be reliably constructed. They can be constructed from a subset of  $M$  data rows, for example a subset constructed by

discarding rows with missing values. After the first-order approximation of Eq. 11 has been built, in particular with a method which allows evaluation of component functions  $f_i(x_i)$  at any  $x_i$  such as RS-HDMR-GPR in the present work (or the previously introduced RS-HDMR-NN<sup>22, 28</sup> where the component functions are fitted with NNs),<sup>18</sup> one can evaluate  $f_i(x_i)$  for any row  $m$  where  $x_i$  is not known:

$$f_i(x_i^m) = f(\mathbf{x}_m) - f_0 - \sum_{\substack{j=1, \\ j \neq i}}^D f_j(x_j^m) \quad (12)$$

from where one imputes

$$x_i^m = f_i^{-1}(y_i^m) \quad (13)$$

where  $y_i^m = f_i(x_i^m)$  is the argument of the inverse function which is now known. If the inverse function  $f_i^{-1}$  is single-valued, i.e. if  $f_i$  is monotonic, this imputation is as good as the first-order HDMR approximation. If the first-order HDMR approximation is very accurate, the imputation can be arbitrarily accurate; in general, it is approximate but can be much more precise than a distribution-based imputation. The component functions  $f_i$  are in general not monotonic; in this case, Eq. 13 results in several alternative choices for  $x_i^m$  and an algorithm is required to pick a choice. The pick may be facilitated if some choices returned by Eq. 13 are deemed to be unrealistic as well as by the use of variable distributions. This will be illustrated in the example below.

If in a given row more than one coordinate value is missing, Eqs. 12, 13 are by themselves insufficient. They could still be used if some missing values are first imputed by other means so that a single missing value per row remained and could be recovered with Eqs. 12, 13. Alternatively, the approach could potentially be extended to a second-order HDMR for pairs of missing variables per row, etc. These more complex cases will not be treated here. Instead, we will show below that Eqs. 12, 13 already provide significant power of imputation of missing entries.

In our implementation, we represent the inverses  $f_i^{-1}$  as a dictionary by subdividing the interval  $[0,1]$  into a specified number  $s$  of evenly spaced subintervals  $[I_i, I_{i+1}]$ , where  $I_i = \frac{i}{s}$  for  $i = 0, 1, \dots, s - 1$ . The dictionary has inputs  $I_i$  for all  $i$ , and the output of each  $I_i$  is a tuple  $(f_1(I_i),$

$f_2(I_i), \dots, f_s(I_i)$ ). In the code, this is stored in a lookup table. Given an output value say  $y_1$ , we select amongst all  $i$  the closest  $f_1(I_i)$  to  $y_1$  and take  $I_i$  as the corresponding input. If we have several  $f_1(I_i)$  values that are all very close to  $y_1$ , say within some threshold distance  $\delta$ , then all of them would be included as candidates. This threshold value is controlled for in the code. If the original functions  $f_i$ 's are not one-to-one, then we are faced with an issue of deciding which input to pick. In fact, there is no way of knowing a priori which input value is correct, as the best choices are application-dependent. By default, we always pick the first candidate in our implementation.

### 3 Examples

We present in this section three examples to demonstrate the use of the RS-HDMR-GPR code and the 1d-HDMR based missing data handler. The first subsection contains an example from chemistry and is the potential energy surface (PES) of  $\text{H}_2\text{O}$ . The second subsection deals with a set of synthetic datasets to demonstrate the use of the 1d-HDMR imputation. Finally, we conclude with a relatively high-dimensional example from quantitative finance.

#### 3.1 Reconstruction of the potential energy surface of $\text{H}_2\text{O}$

In this subsection, we demonstrate the application of the RS-HDMR-GPR algorithm to data encountered in computational chemistry. The dataset sampling the PES of the water molecule consists of 10,001 rows (data points) and 4 columns. The first three columns are the features (in this the two OH bond lengths and the HOH angle), and the last column contains the target, in this case the value of the potential energy (ranging from 0 to 20,000  $\text{cm}^{-1}$ ). The reader is referred to Refs. <sup>6, 22</sup> for the description of the data generation procedures. The data are included in the distribution. The features and the target were linearly scaled to [0,1]. This preserves the distribution of points and non-linear relationships only up to an affine transformation. We train three different models (1d-HDMR-GPR, 2d-HDMR-GPR as per Eq. 3 and a model that fits 2d-HDMR-GPR using linear combinations of the original variables built with the choices of matrices  $A_n$ , that we will call 2d\*-HDMR-GPR), each using 1,000 training points and present the prediction results on the entire dataset of 10,001 points. Each of these models uses 50 self-consistency cycles to train, and each component function is trained with a GPR using a RBF (radial basis function, which is equivalent to squared exponential) kernel of length scale 0.6 and noise variance of  $1 \times 10^{-11}$ . The

scale down parameters used are  $s = 0.1$  and  $e = 1$  (Eq. 9). The coordinate selection matrices for the three models are: for the  $1d$  model,

$$\mathbf{A}_1 = \begin{pmatrix} 1 \\ 0 \\ 0 \end{pmatrix}, \quad \mathbf{A}_2 = \begin{pmatrix} 0 \\ 1 \\ 0 \end{pmatrix}, \quad \mathbf{A}_3 = \begin{pmatrix} 0 \\ 0 \\ 1 \end{pmatrix} \quad (14)$$

for the  $2d$  model,

$$\mathbf{A}_{1,2} = \begin{pmatrix} 1 & 0 \\ 0 & 1 \\ 0 & 0 \end{pmatrix}, \quad \mathbf{A}_{1,3} = \begin{pmatrix} 1 & 0 \\ 0 & 0 \\ 0 & 1 \end{pmatrix}, \quad \mathbf{A}_{2,3} = \begin{pmatrix} 0 & 0 \\ 1 & 0 \\ 0 & 1 \end{pmatrix} \quad (15)$$

and for the  $2d^*$  model,

$$\mathbf{A}_{1,23} = \begin{pmatrix} 1 & 0 \\ 0 & 1 \\ 0 & 1 \end{pmatrix}, \quad \mathbf{A}_{12,3} = \begin{pmatrix} 1 & 0 \\ 1 & 0 \\ 0 & 1 \end{pmatrix}, \quad \mathbf{A}_{13,2} = \begin{pmatrix} 1 & 0 \\ 0 & 1 \\ 1 & 0 \end{pmatrix} \quad (16)$$

The first model implements the approximation  $f(\mathbf{x}) = \sum_{i=1}^3 f_i(x_i)$ , the second,  $f(\mathbf{x}) = \sum_{1 \leq i < j \leq 3} f_{i,j}(x_i, x_j)$ , and the last,  $f(\mathbf{x}) = g_1(x_1, x_2 + x_3) + g_2(x_1 + x_2, x_3) + g_3(x_1 + x_3, x_2)$ . The last model is chosen to illustrate the fact that it may be advantageous to use linear transformations of the original variables.<sup>29</sup>

Their RMSE values on the entire dataset with the three models are, respectively, 462.5, 259.1, and  $52.6 \text{ cm}^{-1}$ . The component functions of the trained models and the correlation plots between the target and the fitted values of the potential energy are shown in Figure 1 and Figure 2, respectively. The shapes first order component functions correspond to a single potential well nature of the fitted function.<sup>30</sup> The shapes of the second order functions also reflect the single-well nature of the fitted function in the interpolation region of the space. The functions reach large values in the corners of the plot as the corners belong to extrapolation regions where there are no data; they correspond to more than one molecular internal coordinate reaching their maximum or minimum values simultaneously, which results in potential energy values beyond the maximum of 20,000 included in the data.<sup>30</sup>

As expected, the second-order model performs better than the first order model. One of the things to note is the improvement in RMSE of the third model compared to the second. Although

they both use  $2d$  component functions, the third model performs significantly better. For dimension  $> 1$ , the inputs of HDMR component functions can be optimized via taking linear combinations of the original inputs, see Ref. <sup>22, 29, 31-33</sup>. This is one of the reasons why we have implemented RS-HDMR-GPR using matrices to determine the input of component functions, even though in the present implementation the linear combinations are not optimized by the code and need to be defined by the user. In Figure 1, we have also plotted the convergence rate of the  $2d^*$  model result on the training set across the self-consistency cycles. The parameters we choose for Eq. (9) are  $s = 0.1, e = 2$ , which ensures that  $a(c) = 1$  on cycle 25 of 50 cycles, to show the fit behavior after the scaling has been removed. This convergence behavior is typical for all presented models.

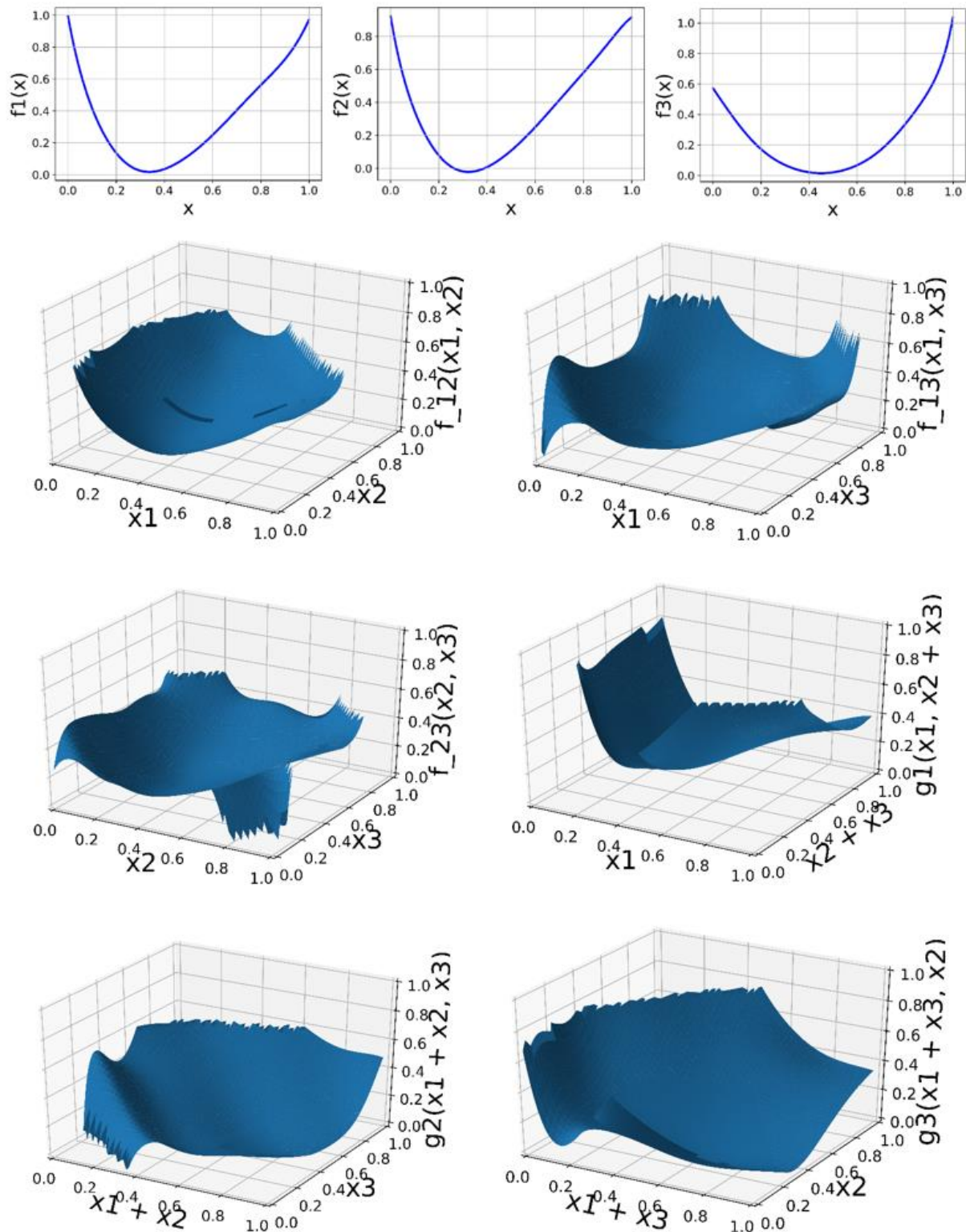


Figure 1. Left to right and top to bottom: the component functions of 1d-HDMR-GPR, the component functions of 2d-HDMR-GPR, and the component functions of 2d\*-HDMR-GPR model of the potential energy surface of H<sub>2</sub>O.

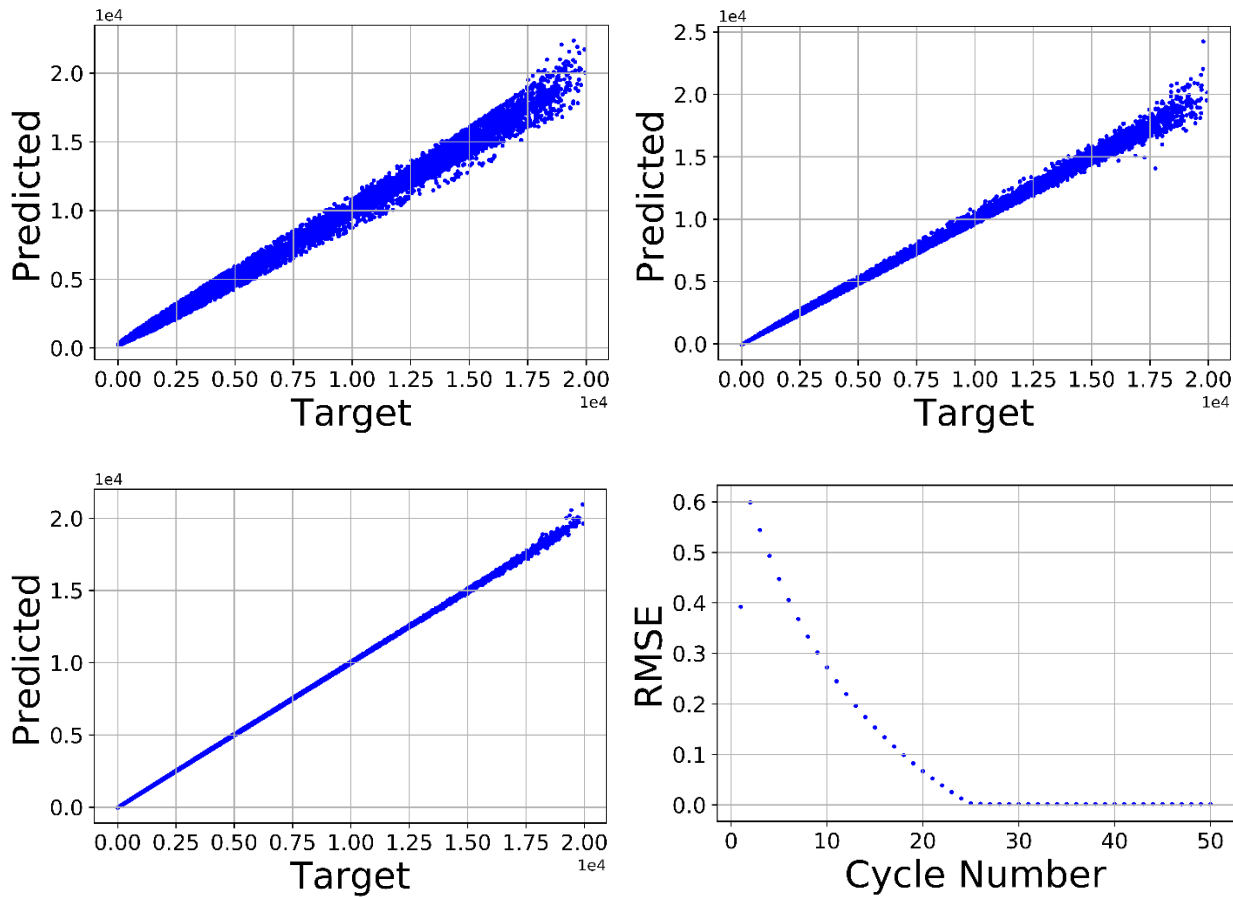


Figure 2. Left to right and top to bottom: predicted vs true values of the  $\text{H}_2\text{O}$  potential energy from 1d-HDMR-GPR, 2d-HDMR-GPR and 2d\*-HDMR-GPR models, and an example of RMSE convergence on the training set over cycles for the 2d\*-HDMR-GPR model.  $a(c)$  of Eq. 9 reaches 1 on cycle  $c = 25$ .

### 3.2 Synthetic datasets

In theory, the 1d-HDMR imputation of a dataset should be perfect when there is no coupling between the variables. We demonstrate this by creating a synthetic dataset using the function  $f(x, y, z) = x + y + z$  for which outputs are known. We generate it using a uniform random generator of 10,000 data entries, for each input variable  $x, y, z$  all of whose values belong to the closed interval  $[0, 1]$ . Our feature matrix  $\mathbf{X}$  will be a  $10,000 \times 3$  matrix (where the columns represent the values of  $x, y$  and  $z$  respectively) and our output vector  $\mathbf{Y}$  is determined by  $f(x, y, z)$ . We scale  $\mathbf{Y}$  so that its components are also within  $[0, 1]$ . Taking 400 rows from the generated dataset, we set 300 aside and randomly assign missing values. The missing values are assigned so that each

row in this set has exactly one missing value, and the missing values are distributed evenly across the columns (i.e. each column has exactly 100 missing values). Using only the remaining 100 points for training a 1d-HDMR model, we obtain an RMSE of 0.0027 upon prediction using the entire dataset. Because of no coupling, in theory we expect almost perfect imputation on the dataset. Indeed, after imputing the 300 points and retraining on all 400 rows, we obtain an RMSE of 0.0028 on the entire dataset. We point out that these reported RMSE values are subject to minor changes when a different random seed is selected. This is the case throughout the rest of this section. We have fixed the random seed in the code, so that the values reported in this document will always be generated. All trainings are done with the RBF kernel and the same hyper-parameters (length scale = 0.6, noise =  $1 \times 10^{-10}$ ). The correlation plots between the imputed values of each column of the feature space  $X$  with the actual values are shown in Figure 3. Their RMSE values are, respectively, 0.00758, 0.00800, and 0.00748.

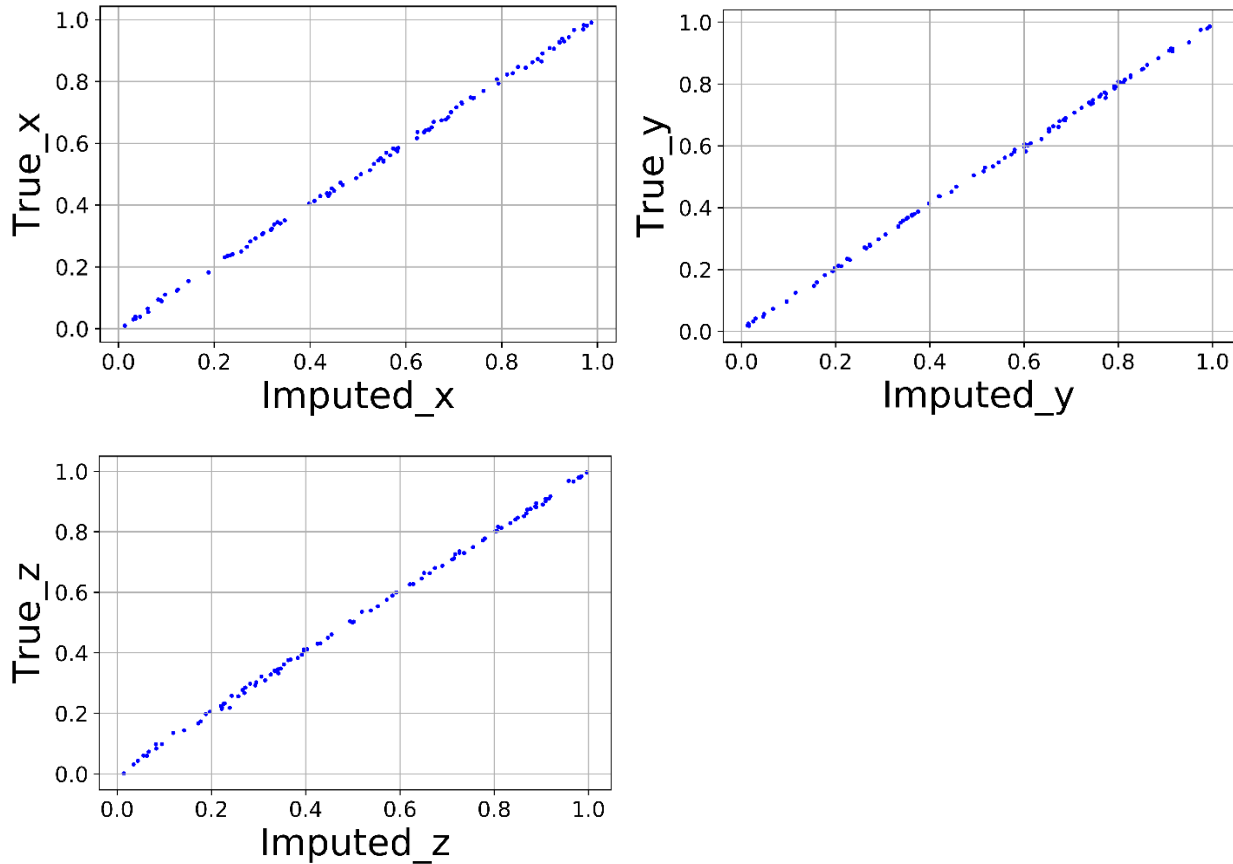


Figure 3. Imputed vs true values of the variables  $x, y, z$  of the function  $f(x, y, z) = x + y + z$  with 1d-HDMR-GPR.

We also point out that for this type of test function, we have also performed tests with data degrades by noise of different levels, increased dimension beyond three, data generated with uneven distributions. All of these factors has an impact on the imputation. To demonstrate this, we have plotted the imputation of the first component for:

1. A 15-dimensional example, i.e.  $f(x_1, x_2, \dots, x_{15}) = x_1 + x_2 + \dots + x_{15}$ . RMSE: 0.018.
2. The 3d example with noise added to the target having a standard deviation of 0.05. RMSE: 0.049.
3. The 3D examples with regenerated features using an uneven distribution appending 10,000 data points generated from a normal distribution generator with  $\mu = 0.1, \sigma = 0.01$  and 5,000 data points from a uniform generator in  $[0, 1]$ . RMSE: 0.014.

For a fair comparison, all of these are trained with 200 points and imputed on 100 points.

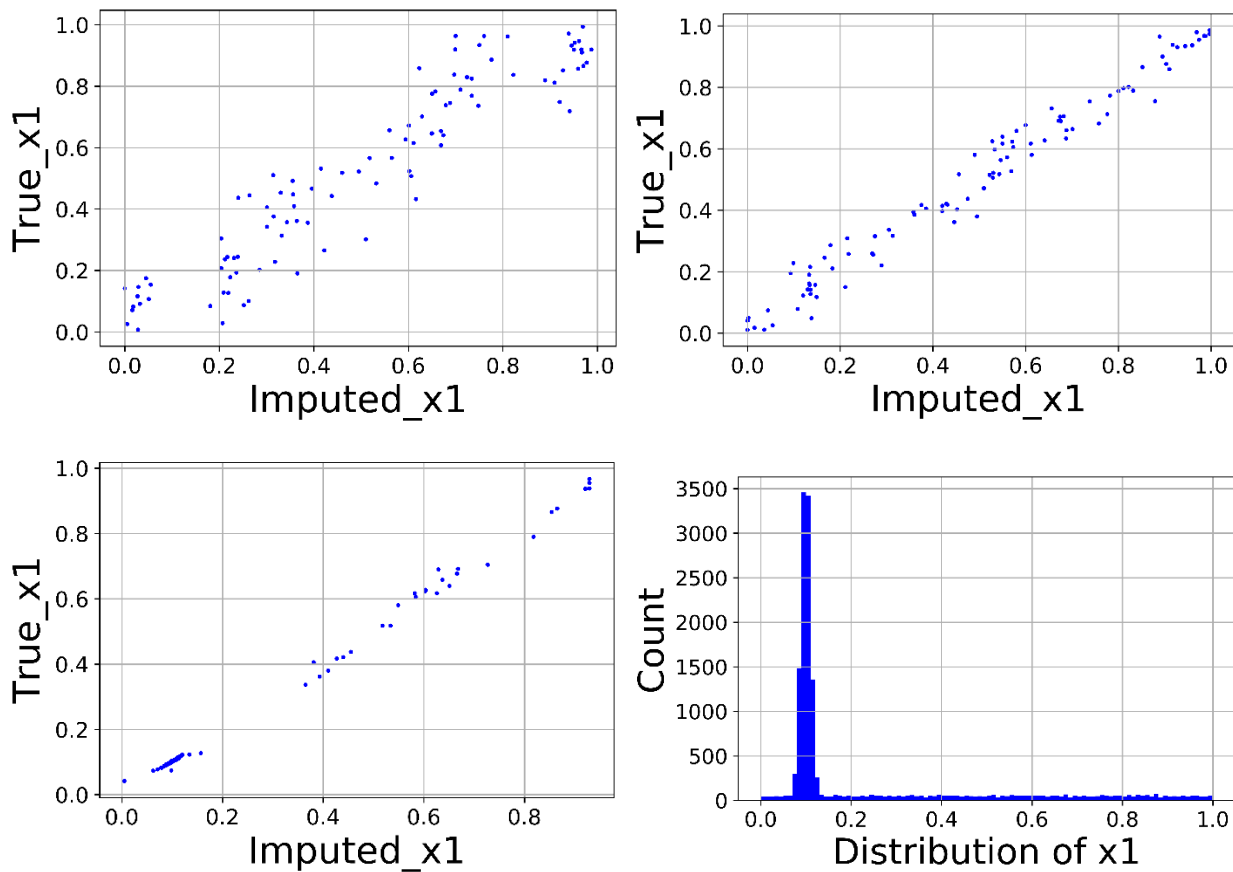


Figure 4. Examples of imputation of missing values of  $x_1$  for a 15-dimnesional example (top left), 3-dimensional example with noise (top right), and a 3-dimensional example with uneven distribution (bottom left) as well as the distribution itself (bottom right).

The results of some of the imputations are shown in Figure 4. We see that depending on the extent of the aforementioned distortions to the function, the data distribution, or noise level, the quality of imputation will be affected. The user is therefore advised to carefully control for these factors. For all the examples in the remainder of this section, unless otherwise stated, are trained on 100 points and imputed on 100 points for each component function.

To demonstrate the effect of singularities of  $f_i^{-1}$  in Eq. 13, we now modify  $f(x, y, z)$  to  $f(x, y, z) = x^3 + y + z^5$ . In this case, we obtain correlation plots shown in Figure 5. Observe that near the origin, the first and third graph imputations are not very accurate. This is due to two reasons. One being that near the origin the functions  $y = x^3$  and  $y = x^5$  are nearly horizontal. The second reason is we are using 1000 subintervals for imputation, so for a neighborhood around the origin the output values are tightly packed together. Hence, for several values, the inverse within a subinterval can be computed to be the same. We can mitigate this issue by using more subintervals, however, the issue will persist within a smaller neighborhood around the origin where the derivative of  $f$  is zero.

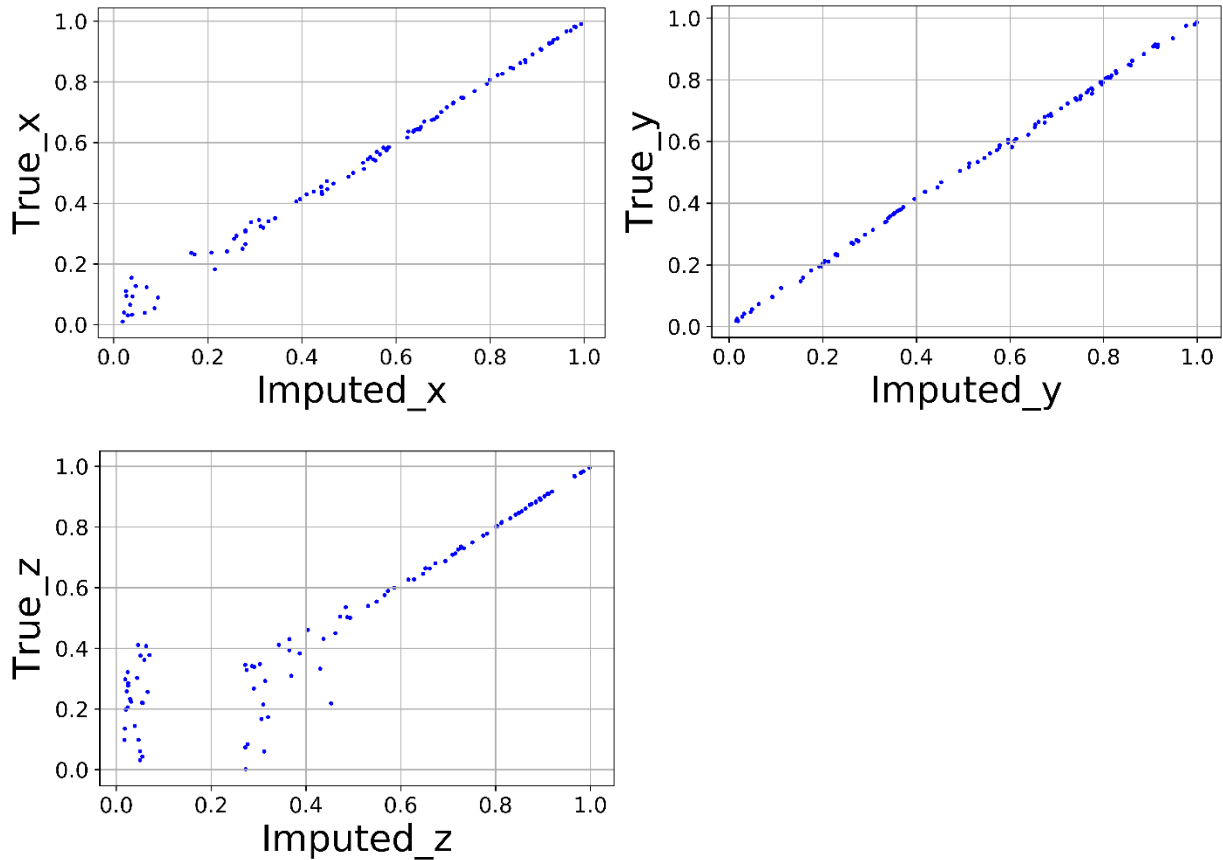


Figure 5. Imputed vs true values of the variables  $x, y, z$  of the function  $f(x, y, z) = x^3 + y + z^5$  with 1d-HDMR-GPR.

To demonstrate the effect of multivaluedness of  $f_i^{-1}$  we use  $y = (x - 0.5)^2$  (again on  $[0, 1]$ ) where the inverse function is not one-to-one. In this case, because the quadratic has two possible values, the correlation plot may look like an “X” or a portion of it. This is expected because the quadratic equation is symmetric about  $x = 0.5$ . Although there are two possible values in this case, we do point out that among the candidates for the imputation, there is always a correct choice. Consider  $f(x, y, z) = 0.5((3.5(x - 0.5))^4 - (5.5(x - 0.5))^2 + 1.6) + y + z$ . The  $x$ -component of this function can be quadruple-valued for  $x$  in  $[0, 1]$ . In Figure 6, we have graphed the possible imputed values with the actual values of the  $x$ -component, using 100 randomly selected points and setting it to missing.

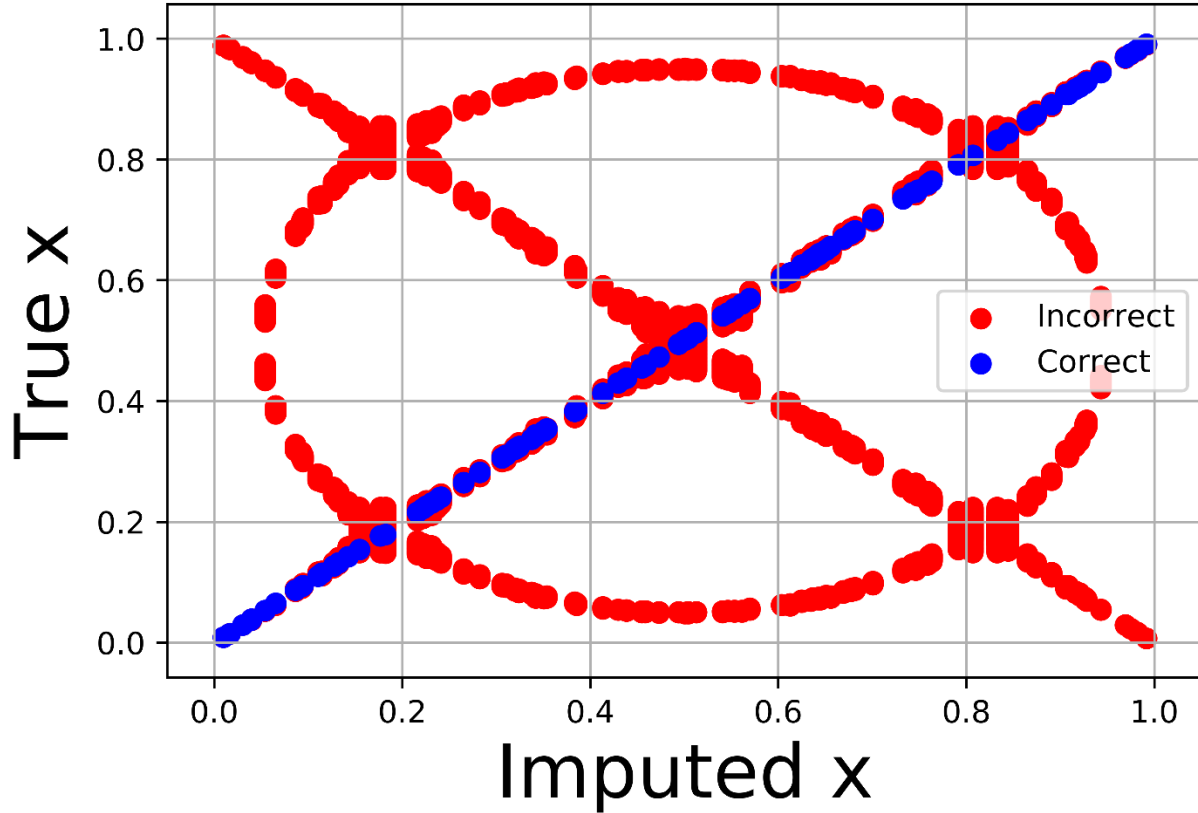


Figure 6. Possible imputed values of  $x$  for  $f(x, y, z) = 0.5((3.5(x - 0.5))^4 - (5.5(x - 0.5))^2 + 1.6) + y + z$ .

The figure shows that the correct choice is always among the candidates provided. In fact, if the model is accurate, it is guaranteed that the there will always be a correct choice among the candidates given. When a component function has multiple local minimums or is flat at certain regions, the imputation is not accurate because of the error in the 1d-HDMR model. It is possible in some cases that the correct value is never considered, due to the fact that the correct candidate maybe be on a flat region of the curve that is at a distance  $\delta$  (that is the size of the error of the 1d-HDMR approximation) away from the value being matched. For example, consider  $g(x) = 0.5((3.5(x - 0.5))^4 - (5.5(x - 0.5))^2 + 1.6)$  and Figure 7.

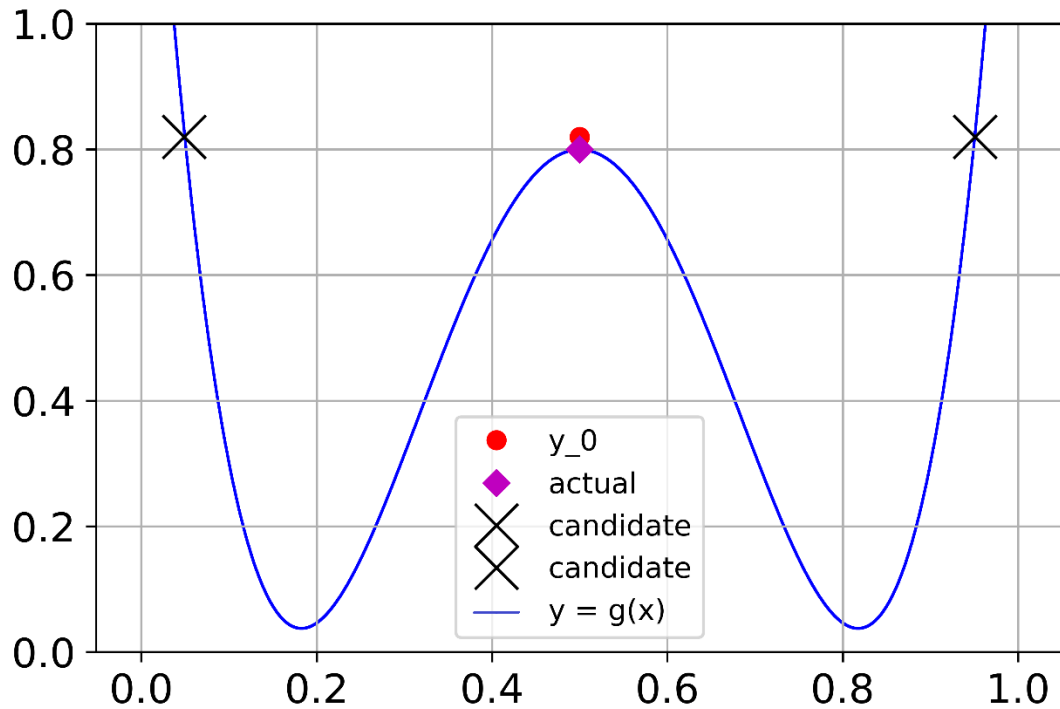


Figure 7. Illustration of a possible effect of the error due to the 1d-HDMR approximation on imputation. The function being illustrated is  $g(x) = 0.5((3.5(x - 0.5))^4 - (5.5(x - 0.5))^2 + 1.6)$ .

The  $y$  coordinate of the red point is the computed output of  $g(x)$ . By our method of imputation, we would end up with the two points marked ‘X’s as the correct candidates. However, the true correct imputation would be the purple diamond point. The distance between the red and purple point is due to the error of the 1d-HDMR model underlying the imputation. From Eq. 12, the computed output of a component function is taken as the difference of the label with the sum of the other component outputs. This implies that the computed output has error at least equal to the error coming from the 1d-HDMR model. To ensure that we can still obtain the actual value, we can set a threshold distance  $\delta$ , so that the candidates within that distance will be considered. However, one should be careful as not to set the threshold to be too high to ensure that the number of candidates to consider remains reasonable. The threshold can be set in the code.

The last synthetic example we use is  $f(x, y, z) = x + 0.2xy + y + z$  to demonstrate the effect of coupling of the inputs. Here  $x$  and  $y$  are correlated. The resulting imputations based on

1d-HDMR, as expected, is less accurate compared to the first example without the  $0.2xy$  term. The resulting RMSE values of the imputations are 0.0188, 0.0172, and 0.0217 for  $x$ ,  $y$ , and  $z$  variable, respectively. The correlation plots are shown in Figure 8. Imputation is reasonable even for coupled variables as long as coupling terms are relatively small (small enough for a reasonable 1d-HDMR approximation). We point out that the variable  $z$ 's imputation accuracy is also affected because of the higher error from the model. The imputation error on any variable will always be at least as large as the error from the model.

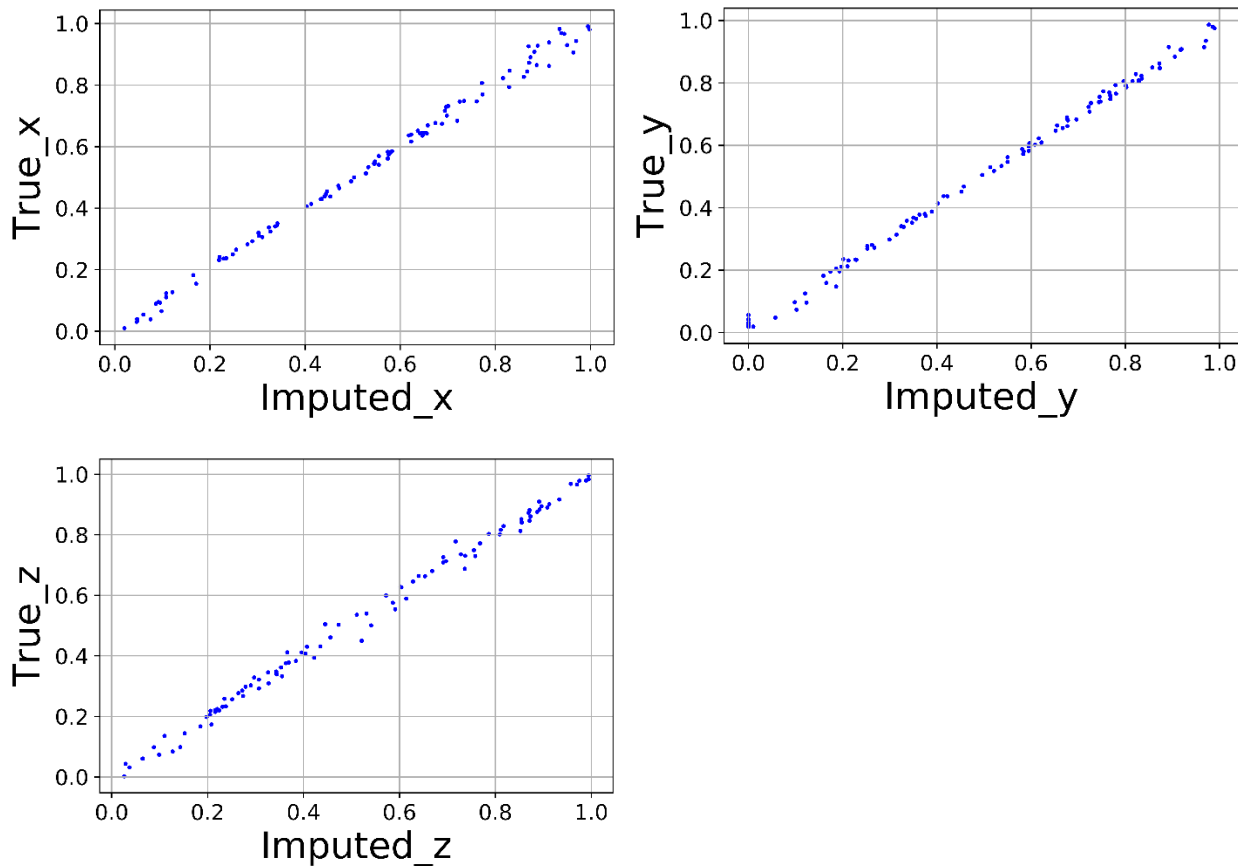


Figure 8. Imputed vs true values of the variables  $x$ ,  $y$ ,  $z$  of the function  $f(x, y, z) = x + 0.2xy + y + z$  with 1d-HDMR-GPR.

### 3.3 Example from quantitative finance

The algorithm RS-HDMR-GPR is general and can be very useful in many applied domains of business and science. Stock market indexes prediction represents a stringent test for making

predictions and imputation. Indeed, stock price time series are often characterized by a chaotic and nonlinear behavior which makes the predictions a challenging task. We demonstrate in this section the use of the algorithm for learning the dependence of S&P 500 index on other financial variables and on imputing missing values in this type of real datasets.

The data were collected for the period of 2001-01-01 to 2020-07-31. To see how S&P 500 is affected by other major world indexes and selected currencies and commodities, we include them as features as described in the last paragraph. The period we consider includes bear and bull markets including some major crashes as well as periods with relatively high and low interest rates. As different data series had different missing dates (weekends, holidays), the total dataset had incomplete rows which were interpolated with splines. We then scaled the data to  $[0, 1]$  to simplify the hyper-parameter tuning of the model. The final data consist of 3927 rows and 15 columns. The first 14 columns represent the feature which includes the time series major financial indexes DAX, Nikkei 225, Nasdaq composite, aggregate US-traded bond index (ticker symbol AGG, ticker symbols refer to the US markets if not states otherwise), and volatility index (VIX); macroeconomic variables money supply M2 and short term rates (exemplified by the 3-months US Treasury bill rate, ticker symbol IRX), and commodities prices such as gold (proxied by the gold bullion ETF, ticker symbol GLD) and oil (proxied by a crude oil ETF traded on TSX, ticker symbol HUC.TO) as well as major currencies the Japanese yen (JPY), the Euro (EUR), the Chinese yuan (CNY), and the Canadian dollar (CNY). IQ Real Return ETF (ticker symbol CPI) is used to include inflation information. The vector of features is  $\mathbf{X} = (\text{CPI}, \text{IRX}, \text{GLD}, \text{HUC.TO}, \text{AGG}, \text{VIX}, \text{N225}, \text{GDAXI}, \text{Nasdaq}, \text{CAD}, \text{JPY}, \text{EUR}, \text{CNY}, \text{M2}, \text{SP500})$ , where the hat is used to signify a market index. We denote by  $\mathbf{x} = (x_1, x_2, \dots, x_{14})$  the feature vector with the elements scaled to  $[0, 1]$ .

After optimizing the model hyper-parameters (the width of the kernel and the noise), the length scale of the isotropic squared exponential covariance function was chosen to be 0.6 and the noise level is in the range of  $10^{-6}$ . Each model uses 50 self-consistency cycles to train. Refitting the financial dataset with RS-HDMR-GPR represents a good test as the dimensionality is relatively high and the data come from the real world and include a random component. The RMSE values on the entire dataset of first, second, and full dimensional RS-HDMR-GPR models are, respectively, 31.6, 14.7, and 16.7. The correlation plots of the predicted vs actual values of the

S&P 500 index are shown in Figure 9 for the  $1d$ -HMDR,  $2d$ -HMDR, and full-D GPR models. One can see that the first order HMDR already obtains a good accuracy.

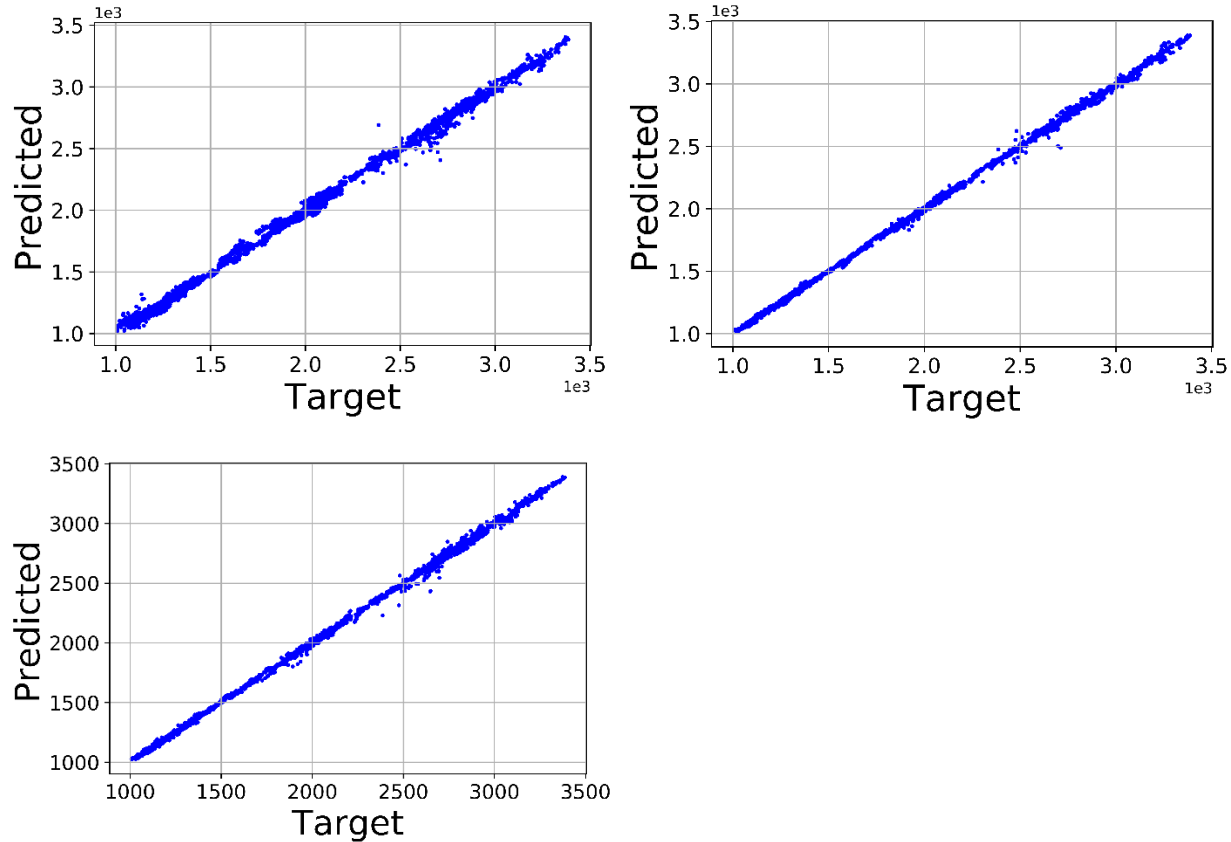


Figure 9. Predicted vs actual values of the S&P 500 index with the  $1d$ -HMDR-GPR,  $2d$ -HMDR-GPR model and the full- $d$ -GPR model.

We now look at the imputation performance for this dataset. To test how well the imputation performs on each column, we pick out the column we want to test, and assign randomly 100 values along that column as missing. As in section 3.2, we need to ensure that only one entry per row is missing. Figure 10 shows examples of two component functions chosen to illustrate cases when the imputation is reliable and unreliable (due to nearly flat regions in the component function). We have chosen the best and the worst (for imputation) variable / component function to illustrate the performance of the imputation. All component functions are shown in the Supporting Information (Figure S1, with imputations shown in Figure S2). The blue points in the imputation plots in Figure 10 illustrate the quality imputation if we selected the best candidates

from the choices provided by Eq. 13. We remind the user that our method does not provide a means of selecting the correct chose but computes a list of possible values and in general guarantees most of the time the correct (closest) choice will be within the list. The blue dots in the picture represents the closest choice to the actual value, while the red dots show other potential candidates. The threshold argument we set for distance  $\delta$  is 0 (i.e. we take into account the case discussed in section 3.2).

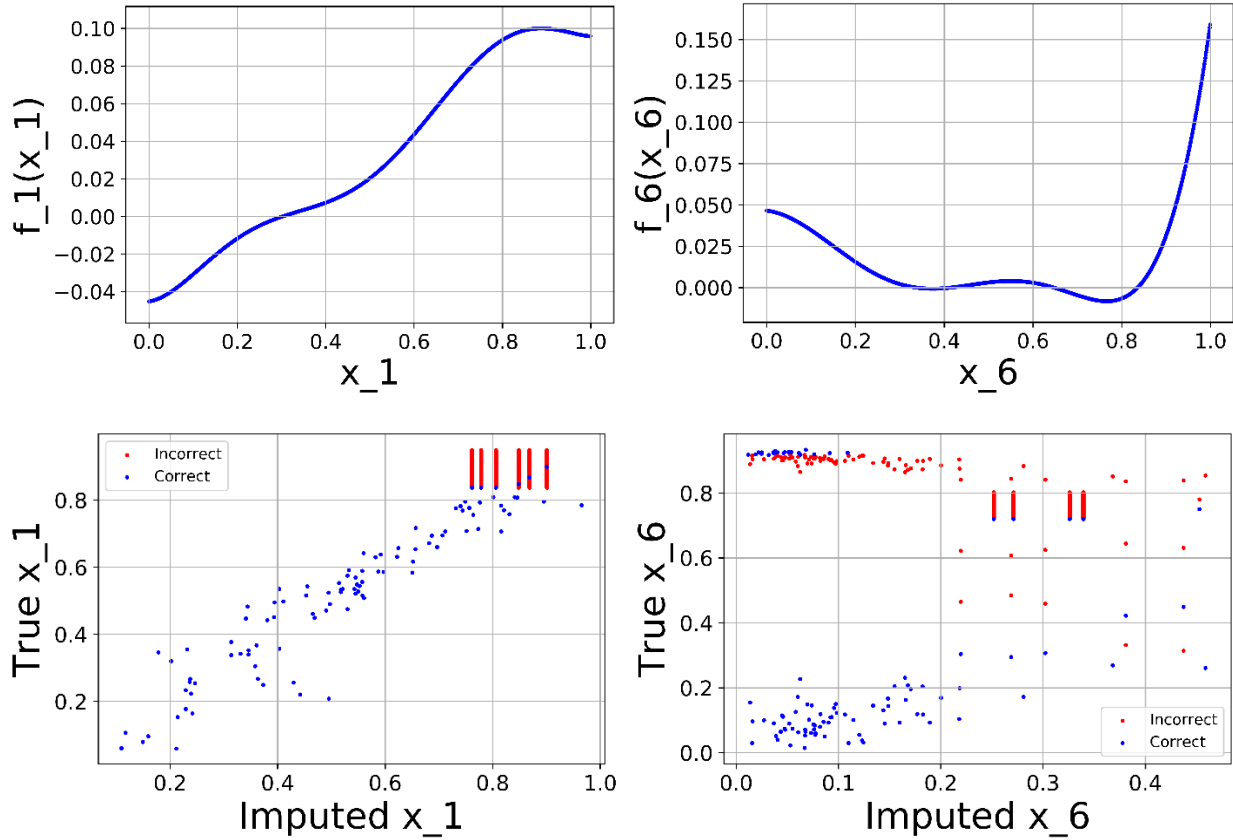


Figure 10. Top row: examples of component functions. Bottom row: imputed vs true values of the corresponding variables.

Assuming the best possible imputation, the RMSE for the worst ( $x_6$  corresponding to VIX) and the best ( $x_1$  corresponding to CPI) cases are, respectively, 0.072 and 0.407. Based on the graphs of the component functions, we expected this to be the case: the more monotonic and less flat curve results in better imputation compared to a flatter and multi-valued function (see section 3.2). The higher errors for the imputation are also due to errors from 1d-HDMR model, and the distributions

of each feature being very uneven which are also factors we explored in the synthetic dataset. Nevertheless, it is in general more precise than conventional methods of imputing such as using the mean of the distribution.

## 4 Conclusions

We presented a Python module that builds approximations to multivariate functions as a sum of lower-dimensional terms of desired dimensionality using the RS-HDMR-GPR approach. The approach is based on the HDMR idea which is expanded to non-orthogonal component functions. The formal expansion over orders of coupling (i.e. including all terms from the 1<sup>st</sup> until the  $d$ -th order) can be dispensed with and instead only functions of a chosen dimensionality  $d$  can be used. The functions are built with Gaussian process regressions. The use of GPR avoids the calculation of multidimensional integrals in the standard HDMR approach. Using lower-dimensional functions allows easier construction of them, in particular, from fewer data. This is particularly important for a method like GPR which scales rather unfavorably with the number of data points. This representation also simplifies the use of the function, in particular, its integration.

The HDMR structure allows for imputation of missing values of variables. Specifically, when only one variable is missing out of  $D$  (in however many data points), and when 1 $d$ -HDMR approximation is reasonable, the imputation can be reliable. In most physical systems, the importance of coupling terms tends to decay rapidly with the order of coupling, so this is expected to be relevant in many practical applications. The imputation quality depends not only on the quality of the 1 $d$ -HDMR model but also on the shape of the component functions: in the absence of flat regions the imputation can be very reliable, while the presence of such regions, compounded by the finite accuracy of the first order model, can make imputation difficult. Nevertheless, the 1 $d$ -HDMR model significantly narrows down possible choices of missing values and should help address this important problem for which substantial generic but accurate approaches are still lacking.

## 5 Acknowledgements

This work was supported in part by National Sciences and Engineering Research Council (NSERC) of Canada and Compute Canada. O. R. is supported by the Mitacs Elevate program.

## 6 References

1. Donoho, D., High-dimensional data analysis: The curses and blessings of dimensionality. In *AMS Conference on Math Challenges of the 21st Century*, AMS: 2000; pp 1-32.
2. *Neural Networks: Tricks of the Trade*. Springer: Berlin, 1998.
3. Manzhos, S.; Dawes, R.; Carrington, T., Neural network based approaches for building high dimensional and quantum dynamics-friendly potential energy surfaces. *International Journal of Quantum Chemistry* **2015**, *115*, 1012-1020.
4. Rasmussen, C. E.; Williams, C. K. I., *Gaussian processes for machine learning*. MIT Press: Cambridge MA, 2006.
5. Golub, P.; Manzhos, S., Kinetic energy densities based on the fourth order gradient expansion: performance in different classes of materials and improvement via machine learning. *Physical Chemistry Chemical Physics* **2019**, *21*, 378-395.
6. Manzhos, S.; Wang, X.-G.; Dawes, R.; Carrington, T., A nested molecule-independent neural network approach for high-quality potential fits. *Journal of Physical Chemistry A* **2006**, *110*, 5295 – 5304.
7. Li, G.; Rosenthal, C.; Rabitz, H., High Dimensional Model Representations. *Journal of Physical Chemistry A* **2001**, *105*, 7765-7777.
8. Alis, O. F.; Rabitz, H., Efficient implementation of high dimensional model representations. *Journal of Mathematical Chemistry* **2001**, *29*, 127-142.
9. Rabitz, H.; Alis, O. F., General foundations of high - dimensional model representations. *Journal of Mathematical Chemistry* **1999**, *25*, 197-233.
10. Fisher, R. A., On the "probable error" of a coefficient of correlation deduced from a small sample. *Metron* **1921**, *1*, 3-32.
11. Sobol, I. M.; Kucherenko, S., Global sensitivity indices for nonlinear mathematical models. Review. *Wilmott* **2005**, *1*, 56-61.
12. Murrell, J. N.; Carter, S.; Frantos, S.; Huxley, P.; Varandas, A. J. C., *Molecular potential energy functions*. Wiley: Toronto, 1984.
13. Carter, S.; Bowman, J. M.; Harding, L. B., Ab initio calculations of force fields for H<sub>2</sub>CN and ClHCN and vibrational energies of H<sub>2</sub>CN. *Spectrochimica Acta A* **1997**, *53*, 1179-1188.
14. Carter, S.; Culik, S. J.; Bowman, J. M., Vibrational self-consistent field method for many-mode systems: A new approach and application to the vibrations of CO adsorbed on Cu(100). *Journal of Chemical Physics* **1997**, *107*, 10458-10469.
15. Carter, S.; Bowman, J. M., Variational calculations of rotational–vibrational energies of CH<sub>4</sub> and isotopomers using an adjusted ab initio potential. *Journal of Physical Chemistry A* **2000**, *104*, 2355-2361.
16. Carter, S.; Handy, N. C., On the representation of potential energy surfaces of polyatomic molecules in normal coordinates. *Chemical Physics Letters* **2002**, *352*, 1-7.
17. Manzhos, S.; Carrington, T., A Random-Sampling High Dimensional Model Representation neural network for building potential energy surfaces. *Journal of Chemical Physics* **2006**, *125*, 084109.
18. Boussaidi, M. A.; Ren, O.; Voitsekhovsky, D.; Manzhos, S., Random Sampling High Dimensional Model Representation Gaussian Process Regression (RS-HDMR-GPR) for multivariate function representation: application to molecular potential energy surfaces. *Journal of Physical Chemistry A* **2020**, *124*, 7598–7607.

19. Li, G.; Hu, J.; Wang, S.-W.; Georgopoulos, P. G.; Schoendorf, J.; Rabitz, H., Random Sampling-High Dimensional Model Representation (RS-HDMR) and orthogonality of its different order component functions. *Journal of Physical Chemistry A* **2006**, *110*, 2474-2485.

20. Wang, S.-W.; Georgopoulos, P. G.; Li, G.; Rabitz, H., Random Sampling-High Dimensional Model Representation (RS-HDMR) with nonuniformly distributed variables: Application to an integrated multimedia/multipathway exposure and dose model for trichloroethylene. *Journal of Physical Chemistry A* **2003**, *107*, 4707-4716.

21. Li, G.; Wang, S.-W.; Rabitz, H., Practical approaches to construct RS-HDMR component functions. *Journal of Physical Chemistry A* **2002**, *106*, 8721-8733.

22. Manzhos, S.; Yamashita, K.; Carrington, T., Fitting sparse multidimensional data with low-dimensional terms *Computer Physics Communications* **2009**, *180*, 2002-2012.

23. Schmitz, G.; Artiukhin, D. G.; Christiansen, O., Approximate high mode coupling potentials using Gaussian process regression and adaptive density guided sampling. *Journal of Chemical Physics* **2019**, *150*, 131102.

24. Li, D.; Tang, H.; Xue, S.; Guo, X., Reliability analysis of nonlinear dynamic system with epistemic uncertainties using hybrid Kriging-HDMR. *Probabilistic Engineering Mechanics* **2019**, *58*, 103001.

25. Kamath, A.; Vargas-Hernández, R. A.; Krems, R. V.; Carrington, T.; Manzhos, S., Neural networks vs Gaussian process regression for representing potential energy surfaces: a comparative study of fit quality and vibrational spectrum accuracy. *Journal of Chemical Physics* **2018**, *148*, 241702.

26. Manzhos, S.; Carrington Jr, T., Neural network potential energy surfaces for small molecules and reactions. *Chemical Reviews* **2021**.

27. Kang, H., The prevention and handling of the missing data *Korean Journal of Anesthesiology* **2013**, *64*, 402–406.

28. Manzhos, S.; Carrington Jr, T., A random-sampling high dimensional model representation neural network for building potential energy surfaces. *Journal of Chemical Physics* **2006**, *125* (8).

29. Manzhos, S.; Carrington, T., Using redundant coordinates to represent potential energy surfaces with lower-dimensional functions. *Journal of Chemical Physics* **2007**, *127*, 014103.

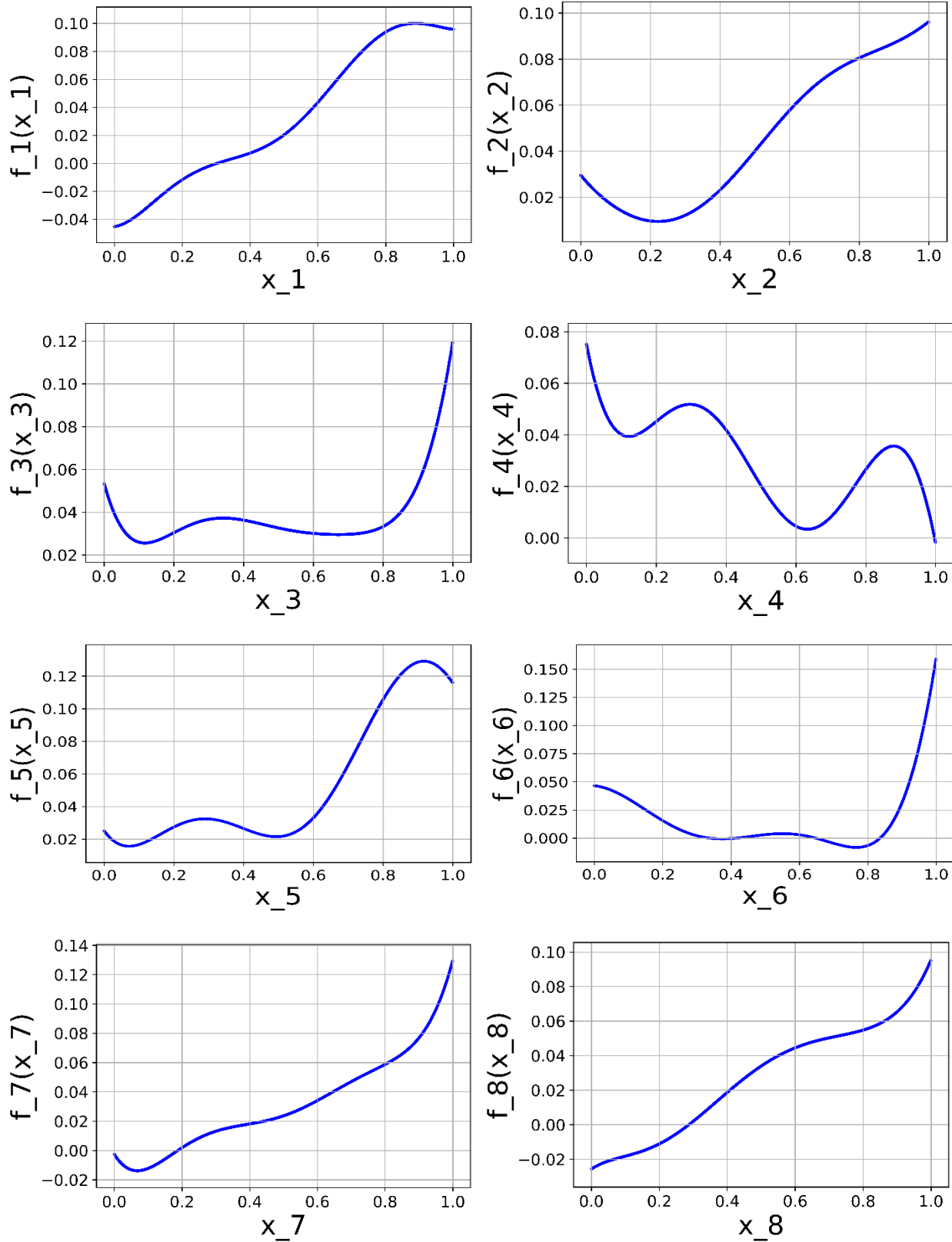
30. Jensen, P. J., The potential energy surface for the electronic ground state of the water molecule determined from experimental data using a variational approach. *Journal of Molecular Spectroscopy* **1989**, *133*, 438-460.

31. Manzhos, S.; Yamashita, K.; Carrington, T., Extracting functional dependence from sparse data using dimensionality reduction: Application to potential energy surface construction. In *Lecture Notes in Computational Science and Engineering*, 2011; Vol. 75 LNCSE, pp 133-149.

32. Manzhos, S.; Yamashita, K., A model for the dissociative adsorption of N<sub>2</sub>O on Cu(100) using a continuous potential energy surface. *Surface Science* **2010**, *604*, 555-561.

33. Manzhos, S.; Nakai, K.; Yamashita, K., Three-body interactions in clusters CO-(pH<sub>2</sub>)<sub>n</sub>. *Chemical Physics Letters* **2010**, *493*, 229-233.

## 7 Supporting Information



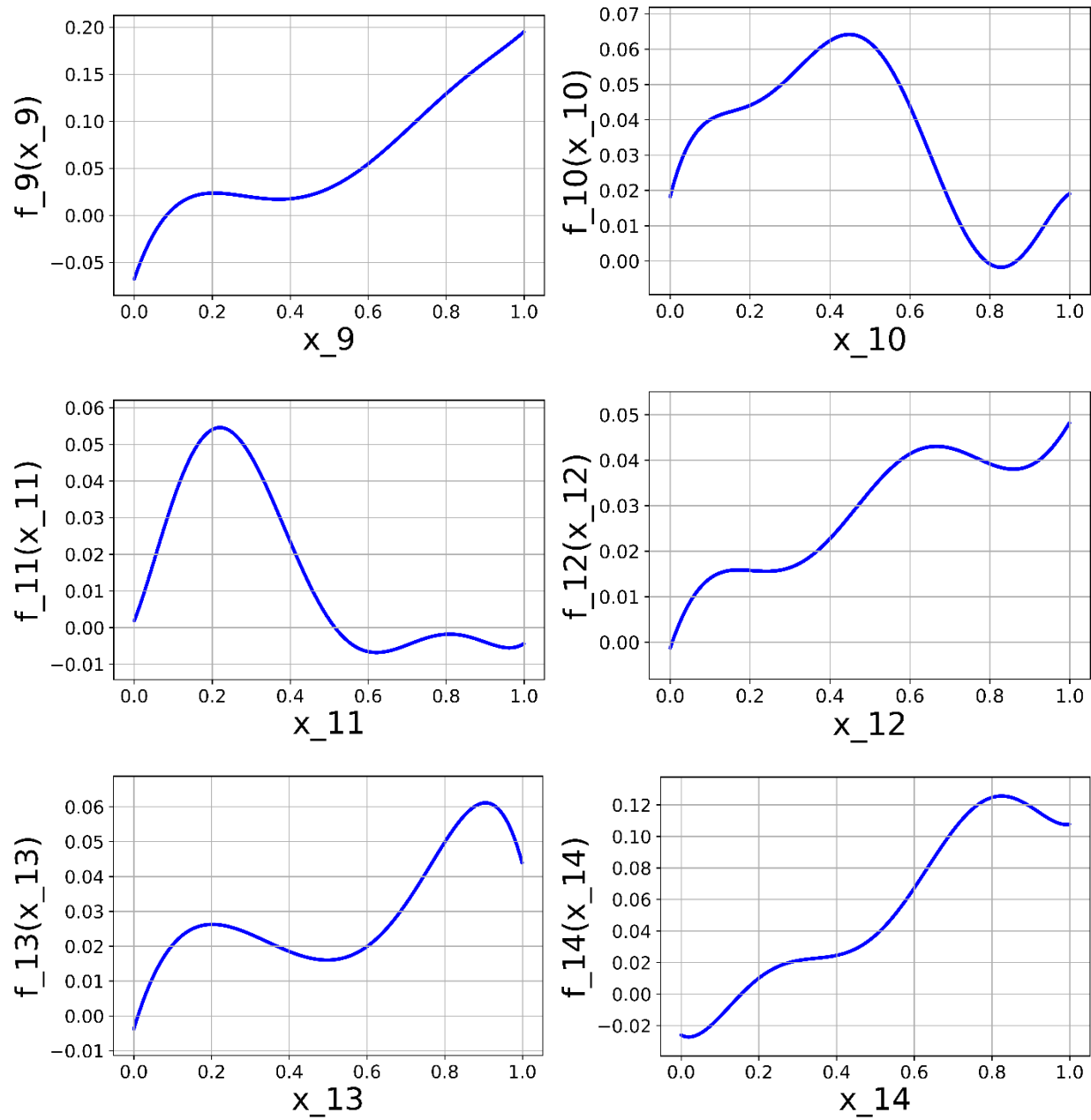
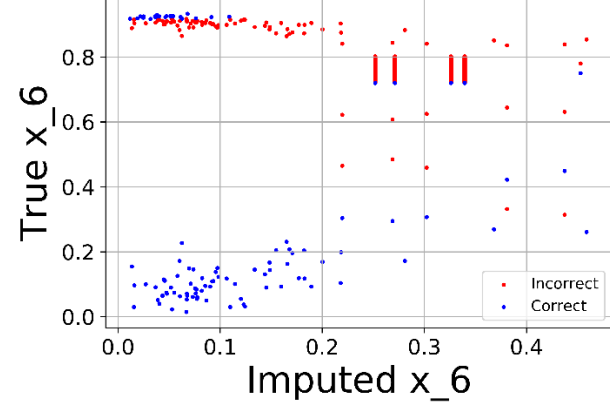
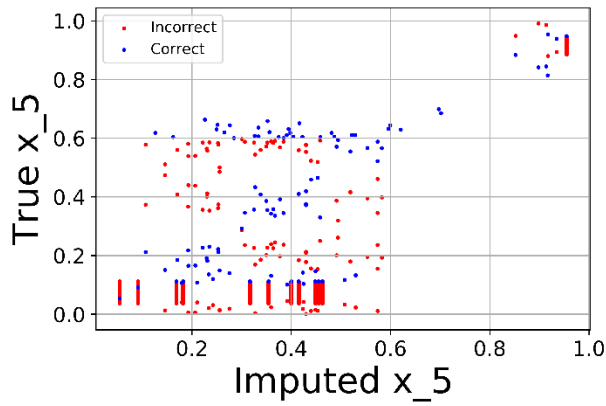
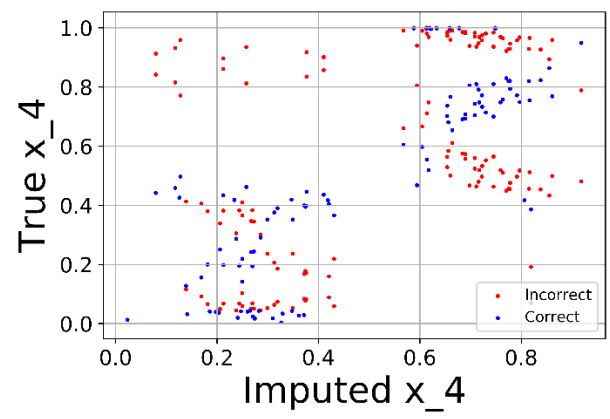
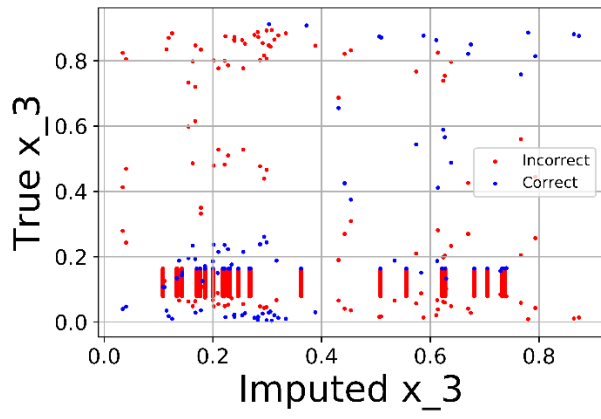
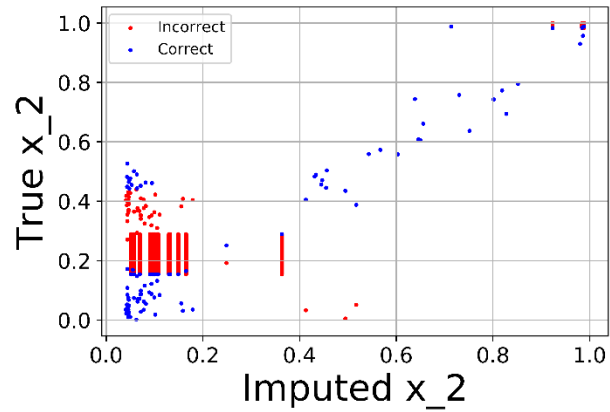
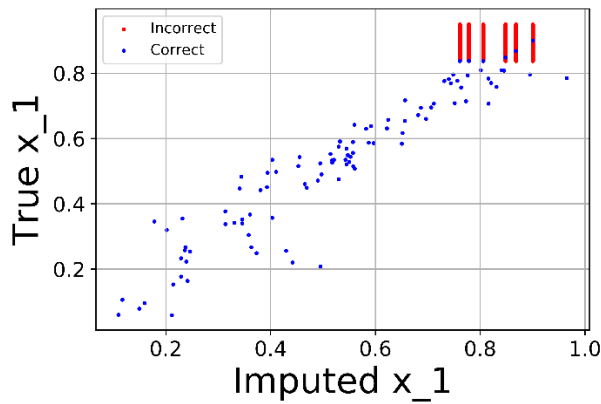


Figure S11. Component functions of the 1d-HDMR-GPR model for the example of section 3.3.



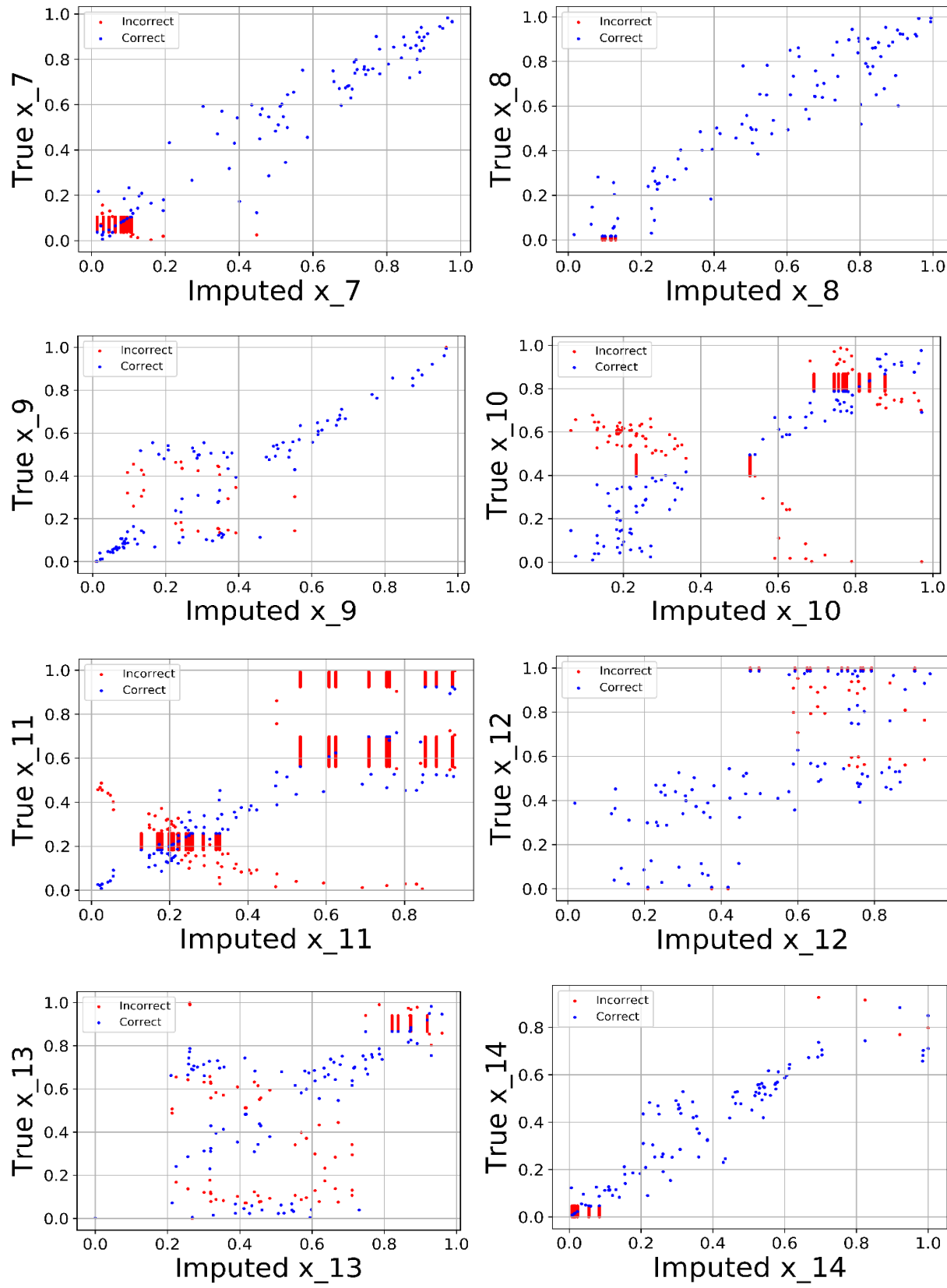


Figure S12. True vs. imputed values of variables for the example of section 3.3.

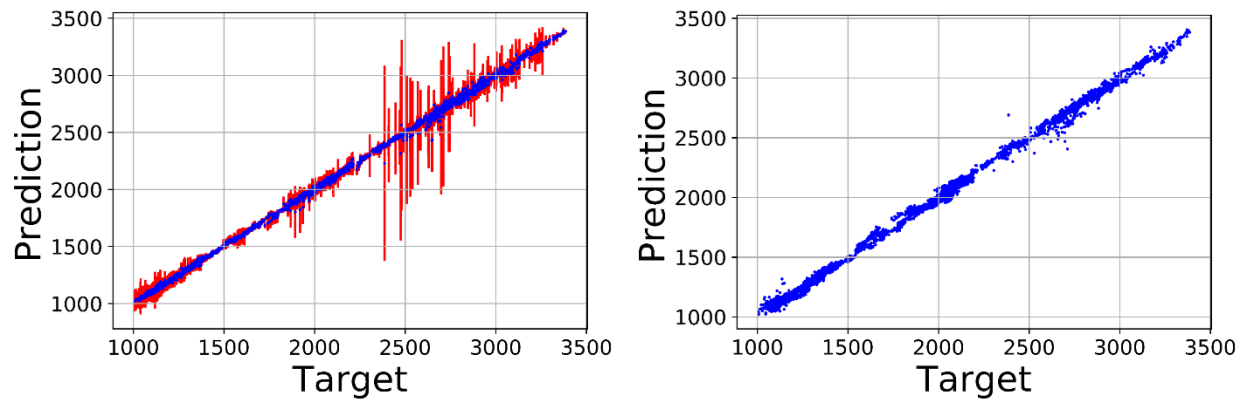


Figure S13. Examples of confidence intervals returned by Eq. 10 in a full-dimensional GPR model and a 1d-HMDR-GPR model for the example of section 3.3. The 1d-HMDR-GPR model has a higher fit RMSE value (31.6 vs 16.7 for the full-dimensional GPR) due to the neglect of coupling, but low confidence intervals (not visible at the scale of the graph) as the 1d component functions themselves are more reliably estimated.